An Improved Proportional Quasi-Resonant Control of Wind Power GCI under Unbalanced Grid Conditions

Xu Deqiang, Jin Zhijian
Department of Electrical Engineering,
Shanghai JiaoTong University, 200240
Shanghai, China
xdq0911@hotmail.com

Abstract: with conventional control strategy under unbalanced grid conditions, power fluctuations will be generated in the input active power and reactive power of the wind power Grid Connected Inverter (GCI). In this paper, a novel sequence extraction method is proposed in the voltage components decomposition. Based on second order generalized integrator (SOGI) with PLL, a decomposition module with an ability of frequency adaptation is built up, called FA-SOGI. To avoid the sequence extraction of grid current, a novel proportional quasi-resonant controller implemented also by FA-SOGI within $\alpha\beta$ stationary coordinate system is introduced to improve inner-loop current control performance. With two objectives of active power fluctuation suppression and reactive power fluctuation suppression, the proposed strategy is verified by simulation and experiment. The results show that the sequence decomposition module is correct and the power fluctuations can be obviously suppressed and DC-bus voltage can be steady.

Key-Words: proportional quasi-resonant (PQR), power fluctuations, unbalanced grid, grid connected inverter (GCI), second order generalized integrator with frequency adaptation (FA-SOGI)

1 Introduction

Nowadays, more and more DFIG-based wind turbines are installed in remote areas or offshore where rural grids are mostly weak and voltage unbalance caused by high power asymmetrical loads, random single-phase loads, and grid faults like short circuit [1, 2]. When wind power grid connected inverters (GCI) work under unbalanced conditions, conventional control strategy, vector-oriented control (VOC), will lead to the appearance of power flow fluctuations, both in the active power and reactive power [3]. The fluctuations of the active power will result in even harmonics in the DC-bus voltage, such as 2, 4, 6 …, which will undermine the performance of the filtering capacitor and its lifetime. Meantime, odd harmonics are generated such as 3, 5, 7… in the AC grid current, thus leaving distortion and unbalance of the input current, including positive and negative components.

Different control schemes have been studied so far to overcome these problems. These include the introduction of negative phase sequence into the current control strategy or the use of the direct power control concept (DPC)[4]. Vector proportional integral (VPI) control is proposed in [2] to eliminate the power flow fluctuations, and reduces the decomposition of sequential components and mathematical complexity. In [5, 6], the authors propose the dual proportional integral (PI) controller in synchronous reference frame, which must introduce the decomposition of positive and negative components with plenty of mathematical calculation. Reference [7] proposes proportional resonant (PR) controller in outer loop to suppress the DC-link ripple and PI repetitive control in the inner loop to eliminate active and reactive power fluctuations. In [8], a strategy of proportional integral (PI) regulator paralleled with a harmonic resonant (R) controller is introduced in the synchronous reference frame.

Proportional resonant (PR) controller introduces an infinite gain at a selected resonant frequency to eliminate steady-state error or current harmonic and thus can regulate sinusoidal variable[9]. Reference [10] discusses the implementation of two different controllers namely proportional-integral (PI) and proportional resonant (PR) controllers in order to obtain the control of grid side converter during single phase to ground fault. References [11-13] introduce PR controller as the current control strategy. As a result, this method improves the performance of the GCI, gets a faster response time and makes the grid current wave more sinusoidal. However, the implementation of these proposed PR controller needs to input a constant value for the resonant frequency,

which will be a drawback in case of grid frequency variation.

During the design of these controllers, a fast and accurate detection of the positive and negative sequence components of the grid voltage is a crucial issue during the design of the controllers, which also determines the quality of the synchronization under polluted and frequency-variable environments. Phase-locked loop (PLL) with filter or notch filter can be used to extract the positive and negative voltage components, however this will result in time delay due to the delay characteristic of the filter. Reference [14] introduces the second order generalized integrator (SOGI) with PLL and proposes a decoupling network called multi-SOGI (MSOGI) based on SOGI-PLL block, but its response can be distorted by inter-harmonics in the input signal [15].

This paper proposes a new method to get the decomposition of voltage components and phase synchronization, which consists of frequency-adaptive cascade SOGI (FA-SOGI) whose frequency follows the fundamental frequency of the grid. For the inner current loop control, a frequency-adaptive proportion integrator controller (FA-PR), which is also based on SOGI, is used to regulate the sinusoidal positive and negative current at the same time. This control scheme is in in $\alpha\beta$ stationary coordinate system, thus avoiding the decomposition of the grid current. Meantime, a notch filter to the sampling DC-bus voltage is included to weaken its oscillatory effect on the whole control system. With the objectives of active power fluctuations suppression or reactive power fluctuations suppression, a 350kW experimental platform is built based on DSP and FPGA system to vary this control scheme.

2 System Model and Control Objective

This paper deals with three phase grid connected inverter (GCI) in wind power system. Note that the zero sequence is ignored in the following discussion as the inverter has a three-phase, three-wire configuration without neutral point connection.

2.1 Model of GCI system

Fig. 1 depicts the configuration of a three-phase wind power GCI. It is assumed that the PWM inverter is supplied by unbalanced input voltages but balanced input impedances. e_a, e_b, e_c are the grid voltage, and i_{ga}, i_{gb}, i_{gc} are the input grid currents. L_g, R_g are the grid filtering inductance, equivalent resistance of transmission line and inductor, respectively. Usually, it is assumed $R_g = 0$ because it is so small that it can be ignored. C is the DC-bus filtering capacitor. u_{dc}, i_{dc}, i_c are DC-bus voltage, DC current and capacitor current, respectively. R_L is DC load, which represents generator side converter.

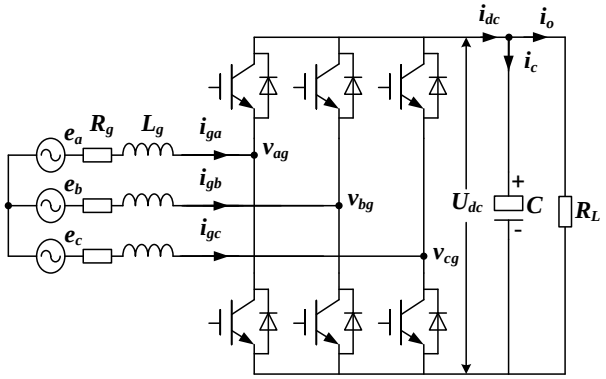

Fig.1 Topological structure of main circuit of grid connected inverters

From Fig.1, a simplified mathematical model can be derived in *dq* synchronous reference frame (SRF) of radian frequency ±ω. The expression is as follows, in which instantaneous variables $f_{dq}{}^p$, $f_{dq}{}^n$ (f= e, u, i) represent the positive and negative components of each variables in SRF.

$$\begin{cases} e_d^p = L_g \dfrac{di_d^p}{dt} + R_g i_d^p - \omega L_g i_q^p + u_d^p \\ e_q^p = L_g \dfrac{di_q^p}{dt} + R_g i_q^p + \omega L_g i_d^p + u_q^p \\ e_d^n = L_g \dfrac{di_d^n}{dt} + R_g i_d^n + \omega L_g i_q^n + u_d^n \\ e_q^n = L_g \dfrac{di_q^n}{dt} + R_g i_q^n - \omega L_g i_d^n + u_q^n \end{cases} \quad (1)$$

$$C\frac{du_{dc}}{dt} = i_{dc} - \frac{u_{dc}}{R_L} \quad (2)$$

The input instantaneous apparent power across the inverter is

$$S = (e^{j\omega t}e_{dq}^p + e^{-j\omega t}e_{dq}^n)\overline{(e^{j\omega t}i_{dq}^p + e^{-j\omega t}i_{dq}^n)} \quad (3)$$

It can be simplified as

$$\begin{cases} p(t) = p_0 + p_{c2}\cos(2\omega t) + p_{s2}\sin(2\omega t) \\ q(t) = q_0 + q_{c2}\cos(2\omega t) + q_{s2}\sin(2\omega t) \end{cases} \quad (4)$$

And it can be expanded in matrix as

$$\begin{bmatrix} p_0 \\ p_{c2} \\ p_{s2} \\ q_0 \\ q_{c2} \\ q_{s2} \end{bmatrix} = \frac{3}{2}\begin{bmatrix} e_d^p & e_q^p & e_d^n & e_q^n \\ e_d^n & e_q^n & e_d^p & e_q^p \\ e_q^n & -e_d^n & -e_q^p & e_d^p \\ e_q^p & -e_d^p & e_q^n & -e_d^n \\ e_q^n & -e_d^n & e_q^p & -e_d^p \\ -e_d^n & e_q^n & e_d^p & e_q^p \end{bmatrix}\begin{bmatrix} i_d^p \\ i_q^p \\ i_d^n \\ i_q^n \end{bmatrix} \quad (5)$$

From (5), besides average active power p_0 and average reactive power q_0 under unbalanced grid condition, there are oscillatory harmonic components that are twice the fundamental frequency—active power harmonic p_{c2}, p_{s2}, and reactive power harmonic q_{c2}, q_{s2}. The second harmonic is primarily result of the interaction between the positive sequence inverter voltage and negative sequence current that flows on the ac-side due to the system unbalance[16].

As (5) shows, it is a four-freedom equation and the four free variables are i_d^p, i_q^p, i_d^n, i_q^n. However the variables to control are six ones, including p_0, q_0, p_{c2}, p_{s2}, q_{c2} and q_{s2}. Usually, average active power p_0 and average reactive power q_0, are under control. In addition, the active power oscillatory harmonic components or the reactive ones can be under control, too.

With the active and reactive power reference values, the current reference values can be calculated, including both positive sequence current and negative sequence current. From the analysis above, we can get two different control objectives as follows.

2.2 Control objective: active power fluctuations suppression

When the wind power generation system is working under unity power factor, the generator delivers active power to grid. In order to protect DC-bus capacitor and keep DC-bus voltage steady, the active power fluctuations should be suppressed. Therefore, $p_{c2} = p_{s2} = 0$, and the positive and negative current reference value is

$$\begin{bmatrix} i_d^p \\ i_q^p \\ i_d^n \\ i_q^n \end{bmatrix} = \frac{2p_0}{3D_1}\begin{bmatrix} e_d^p \\ e_q^p \\ -e_d^n \\ -e_q^n \end{bmatrix} + \frac{2q_0}{3D_2}\begin{bmatrix} e_q^p \\ -e_d^p \\ e_q^n \\ -e_d^n \end{bmatrix} \tag{6}$$

where, $\begin{cases} D_1 = [(e_d^p)^2 + (e_q^p)^2] - [(e_d^n)^2 + (e_q^n)^2] \\ D_2 = [(e_d^p)^2 + (e_q^p)^2] + [(e_d^n)^2 + (e_q^n)^2] \end{cases}$

2.3 Control objective: reactive power fluctuations suppression

When grid voltage sags happen, the wind generation system need to compensate or absorb reactive power. For this scenario, the reactive power oscillatory harmonic should be suppressed. Therefore, $q_{c2} = q_{s2} = 0$; the positive and negative current reference value is

$$\begin{bmatrix} i_d^p \\ i_q^p \\ i_d^n \\ i_q^n \end{bmatrix} = \frac{2p_0}{3D_2}\begin{bmatrix} e_d^p \\ e_q^p \\ -e_d^n \\ -e_q^n \end{bmatrix} + \frac{2q_0}{3D_1}\begin{bmatrix} e_q^p \\ -e_d^p \\ e_q^n \\ -e_d^n \end{bmatrix} \tag{7}$$

where D_1 and D_2 are the same with (6).

3 Voltage Components Extraction Based on FA-SOGI

To get the current reference value in (6) (7), positive and negative components of the grid voltage need to be extracted from sampling grid voltage. According to the method of symmetrical components, the positive and negative components can be expressed as

$$\begin{bmatrix} e_a^p \\ e_b^p \\ e_c^p \end{bmatrix} = \frac{1}{3}\begin{bmatrix} 1 & a & a^2 \\ a^2 & 1 & a \\ a & a^2 & 1 \end{bmatrix}\begin{bmatrix} e_a \\ e_b \\ e_c \end{bmatrix} = T^+\begin{bmatrix} e_a \\ e_b \\ e_c \end{bmatrix} \tag{8}$$

$$\begin{bmatrix} e_a^p \\ e_b^p \\ e_c^p \end{bmatrix} = \frac{1}{3}\begin{bmatrix} 1 & a^2 & a \\ a & 1 & a^2 \\ a^2 & a & 1 \end{bmatrix}\begin{bmatrix} e_a \\ e_b \\ e_c \end{bmatrix} = T^-\begin{bmatrix} e_a \\ e_b \\ e_c \end{bmatrix} \tag{9}$$

where $a = e^{j\frac{2\pi}{3}}$ is transformation factor. Through coordinate transformation, (8) and (9) can be expressed in $\alpha\beta$ stationary coordinate system as

$$\begin{bmatrix} e_a^p \\ e_\beta^p \end{bmatrix} = \frac{1}{2}\begin{bmatrix} 1 & -S \\ S & 1 \end{bmatrix}\begin{bmatrix} e_\alpha \\ e_\beta \end{bmatrix} \tag{10}$$

$$\begin{bmatrix} e_a^n \\ e_\beta^n \end{bmatrix} = \frac{1}{2}\begin{bmatrix} 1 & S \\ -S & 1 \end{bmatrix}\begin{bmatrix} e_\alpha \\ e_\beta \end{bmatrix} \tag{11}$$

where $S = e^{-j\frac{\pi}{2}}$ is phase delay factor, which can be realized with second order generalized integrator (SOGI). The structure of SOGI is as Fig. 2 shows.

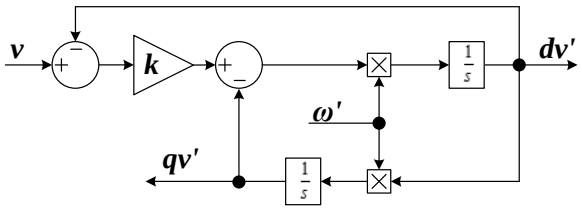

Fig.2 Structural diagram of the proposed SOGI

Fig.2 depicts the structural diagram of a SOGI block. ***v*** is the input signal, and ***dv'*** and ***qv'*** are the in-phase output and quadrature-phase output, respectively. The output signals are mutual perpendicular. The transfer function of the two in-quadrature output of the SOGI are

$$\begin{cases} D(s) = \dfrac{d(s)}{v(s)} = \dfrac{k\omega_0 s}{s^2 + k\omega_0 s + \omega_0^2} \\ Q(s) = \dfrac{q(s)}{v(s)} = \dfrac{k\omega_0^2}{s^2 + k\omega_0 s + \omega_0^2} \end{cases} \tag{12}$$

where ***k*** is the damping factor, and ω_0 is the resonant frequency. The output signals' magnitude and phase are expressed in (13) and (14), and the frequency response of the transfer function is shown in Fig.3.

$$d = Dv \begin{cases} |D| = \dfrac{k\omega_0\omega}{\sqrt{(k\omega_0\omega)^2 + (\omega_0^2 - \omega^2)^2}} \\ \angle D = \tan^{-1}\left(\dfrac{\omega_0^2 - \omega^2}{k\omega_0\omega}\right) \end{cases} \quad (13)$$

$$q = Qv \begin{cases} |Q| = \dfrac{k\omega_0^2}{\sqrt{(k\omega_0\omega)^2 + (\omega_0^2 - \omega^2)^2}} \\ \angle Q = \angle D - \dfrac{\pi}{2} \end{cases} \quad (14)$$

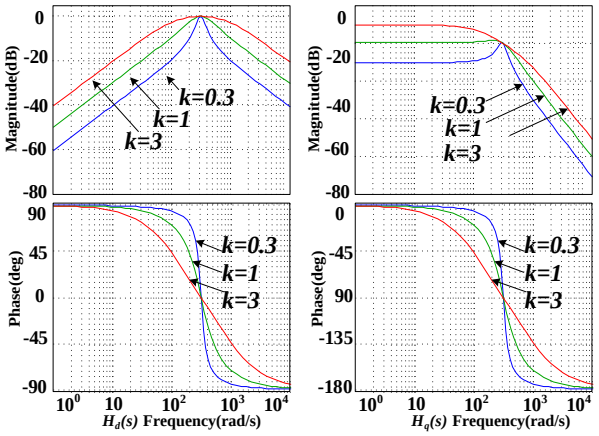

Fig.3 Bode diagram of the SOGI when k varies

As Fig. 3 shows, the SOGI behaves as a band-pass filter (BPF) for ***dv'*** and as a low-pass filter (LPF) for ***qv'***. The attenuation speed of BPF for non-resonant frequency is -20dB and phase shift is zero at ω_0. The attenuation speed of LPF for above-resonant frequency is -40dB and phase shift is -90 degree at ω_0. When damping factor ***k*** varies, it can regulate the bandwidth of the SOGI. Moreover, the bandwidth of the BPF is independent of the resonant frequency, being exclusively set by ***k***, and ***qv'*** is always 90 degree lagged from the ***dv'***[17].

With (10) and (11), the positive component and negative components can be extracted from grid voltage. Then the positive components can be used in PLL for the synchronization detection. As Fig.4 shows, the extracted positive components are the input signals of PLL. Moreover the detected synchronization phase is the input signal for SOGI, in turn, which make SOGI frequency-adaptive when grid frequency oscillation happens, resulting in frequency adaption SOGI block (FA-SOGI).

With the FA-SOGI block, the 3rd positive and negative sequence components can be also extracted from grid voltage. On this occasion, the resonant frequency of FA-SOGI is 3 times fundamental frequency, namely 150Hz, and damping factor is tuned as needed. So does the 5th positive and negative sequence components or other Nth (N=3, 5, 7...) components.

In order to get greater harmonic attenuation speed for filtering performance and faster response time, another SOGI block is added into FA-SOGI to prefilter the non-resonant component [15].

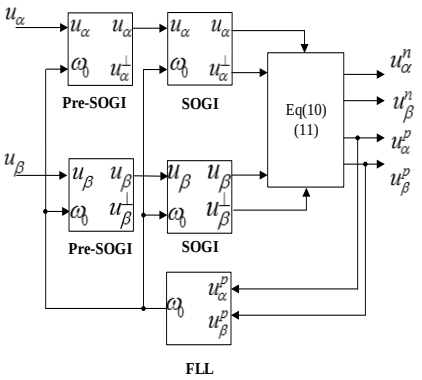

Fig.4 Structural diagram of fundamental components detection with FA-SOGI

4 Design of System Controller

The control strategy applied in this paper for wind power generation GCI mainly consists of dual closed loops. The external loop is voltage loop which controls the DC-bus voltage, while the inner loop is current loop which regulates grid current. The voltage loop is responsible for balancing the active power flow and system stability. And the current loop works for power quality and current unbalance. The whole control system is showed in Fig.6.

4.1 Design of voltage loop controller

The closed voltage loop is to keep the active power steady, and to suppress the dc voltage ripple. This is implemented through a proportional integrator (PI) as follows,

$$p_0^* = i_{dc}^* U_{dc}^* = [(k_{up} + \frac{k_{ui}}{s})(U_{dc}^* - U_{dc})]U_{dc}^* \quad (15)$$

where p_0^* is the active power reference injected by the grid, which is used to calculate the inner current reference in (6) and (7). In addition, when the GCI is working under unity power factor, the reactive power reference q_0^* is zero. Otherwise, when the GCI is injecting or adsorbing reactive power, q_0^* could be a nonzero constant, which can be assigned directly or indirectly through power factor.

4.2 Design of the current loop controller

The PR controller is based on the internal principle mode so that a sinusoidal reference with frequency ω_0 can be tracked without steady state error [18]. Taking consideration in that, it could be used in $\alpha\beta$ stationary coordinate system. The transfer function of PR is as follows,

$$G_{PR} = k_p + \frac{k_i s}{s^2 + \omega_0^2} \tag{16}$$

It is known that the bandwidth of the resonant controller is extremely narrow, which make it possible for whole system unsteady when working under a slight variation on frequency. Therefore, an improved proportional quasi-resonant (PQR) controller is proposed [18], and its transfer function is

$$G_{PR} = k_{ip} + \frac{2k_{ii}\omega_c s}{s^2 + 2\omega_c s + \omega_0^2} \tag{17}$$

Attention should be paid that the application of quasi-resonant (QR) needs to tune the resonant frequency especially when grid frequency variation occurs, however it is difficult for this conventional PQR controller. Therefore it is desirable that the resonant frequency ω_0 could be tuned automatically with the grid frequency varies, which is a frequency-adaptive PQR (FA-PQR).

From the structure of SOGI, we know the transfer function of SOGI is very alike with that of QR. It is possible to change the structure of SOGI for the implement of PQR, as Fig.5 shows. The input resonant frequency ω_0 is the grid frequency which is detected from FA-SOGI.

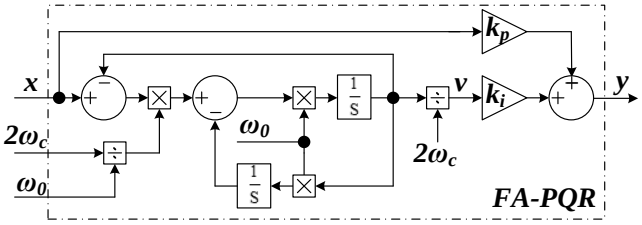

Fig. 5 Block diagram of FA-PQR regulator

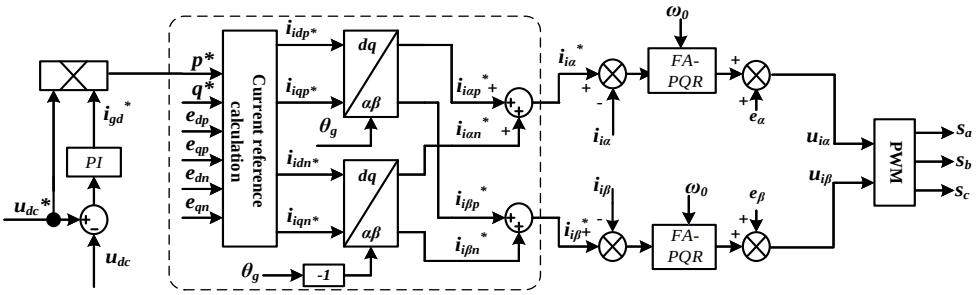

Fig.6 Block diagram of VSC control based on FA-SOGI and FA-PQR controller

5 Simulation and Experimental Results

5.1 Simulation results of FA-SOGI

In order to validate the positive and negative voltage sequence decomposition with FA-SOGI, a three-phase unbalanced grid model is built with Simulink. The fundamental positive sequence voltage is 690V, and magnitude percentages of the positive and negative sequence harmonics is as Tab 1 shows.

Tab 1 configuration of components in simulation

Parameter	Value[pu]
1st P-sequence e_{abcp1}	1
1st N-sequence e_{abcn1}	-0.30
3rd P-sequence e_{abcp3}	0.20
3rd N-sequence e_{abcn3}	-0.15
5th P-sequence e_{abcp5}	0.15
5th N-sequence e_{abcn5}	-0.10

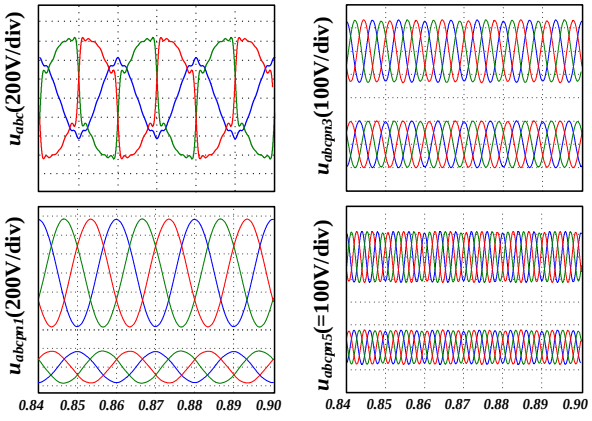

Fig.7 simulation wave of unbalanced grid and the decomposed positive and negative harmonic components

It is seen from Fig.7 that the grid voltage is distorted and unbalanced when it involves positive and

negative sequence harmonic components. As expected, after extracted with the FA-SOGI, the fundamental positive sequence is sinusoidal, the total harmonic distortion (THD) is less than 1.2%, and the magnitude error is less than 0.6%. The other components and relative magnitude error is as Tab 2 shows.

Tab 2 simulation result

Parameter	Magnitude error	THD
1st P-sequence e_{abcp1}	0.60%	1.20%
1st N-sequence e_{abcn1}	2.96%	1.80%
3rd P-sequence e_{abcp3}	5.00%	0.03%
3rd N-sequence e_{abcn3}	10.0%	0.10%
5th P-sequence e_{abcp5}	15.0%	0.32%
5th N-sequence e_{abcn5}	6.60%	0.37%

Tab 2 shows that, compared with injected components, the magnitude of fundamental positive and negative sequence components are accurate and waveform is clean, which reaches the requirement of inner loop current regulation. The error of third positive sequence and the fifth negative sequence harmonics are rather low, while the error of third negative sequence and the fifth positive sequence harmonics are little high, which can be improved by the tuning of the damping factor.

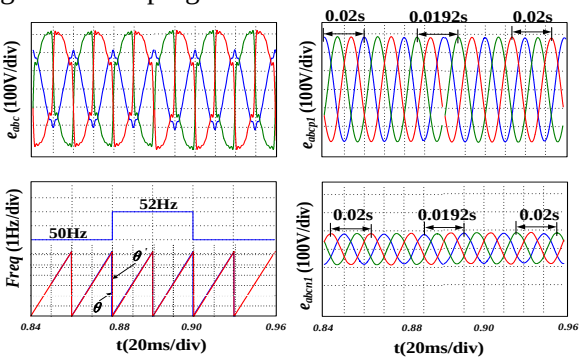

Fig.8 fundamental positive and negative waves when frequency varies

Fig.8 shows the performance of PLL based on FA-SOGI. The frequency varies from 50Hz to 52Hz at t=0.88s, and the detected phase has a small error with the grid reference frequency in this dynamic variation. However, the state error becomes zero within two cycles. The frequency drops from 52Hz to50Hz at t=0.90s, and the performance is as good as the above rising one. The results both show the dynamic response time is smaller than two cycles, namely, 0.04s. The decomposed fundamental positive and negative sequence voltages also have an oscillation but return to normal soon.

5.1 Experimental results

Tab 3 the system configuration in experiment

Parameter	Value	Parameter	Value
AB voltage e_{ab}/V	143	Grid frequency f_0/Hz	50
BC voltage e_{bc}/V	54	DC-bus voltage u_{dc}*/V	400
CA voltage e_{ca}/V	143	Line resistance R_g/mΩ	0.1
Load resistance R_L/Ω	20	DC-bus capacitor C/mF	18.8
line inductance L_g/μH	600	Switch frequency f_s/Hz	3000

Different experiments have been carried out to prove the performance of the FA-PQR control scheme with above two control objectives. The experimental platform's power level is 350kW, and controller chip is floating point type DSP TMS 320C6747/OMAP-L137. The pulses are fired by FPGA xc6slx45. The analog sampling signals are transformed into digital by A/D7656. The unbalanced grid is obtained through two paralleled power transformers. The configuration of the unbalanced grid is as Tab.3 shows.

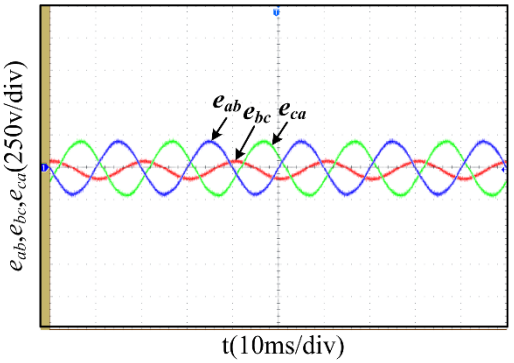

Fig. (10-a) Experimental waveform of unbalanced grid

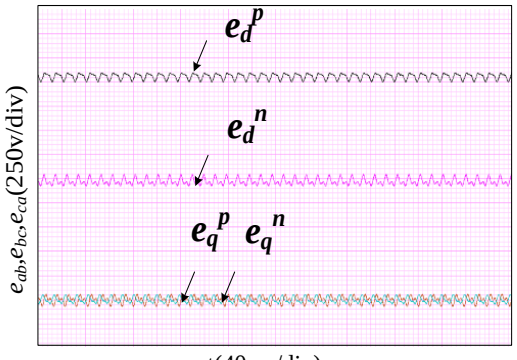

Fig. (10-b) Experimental results of decomposed grid

As Fig. (10-a) shows, the waveform of the grid is unbalanced in magnitude and without phase-shift distortion, under which the GCI works. The phase BC line voltage is 89V smaller than the other two phases. Fig. (10-b) shows the fundamental positive sequence component and negative sequence component in *dq* synchronous reference frame. The waveform is steady only with high harmonic ripples of small mag-

nitude, and the 100Hz harmonics are totally eliminated by the FA-SOGI. This distinguished performance of FA-SOGI highlights the features of elimination $2f_0$ pulsations.

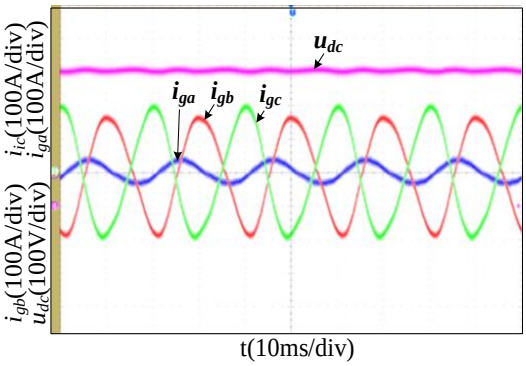

Fig. (11-a) wave of i_{abc} and u_{dc} at steady state

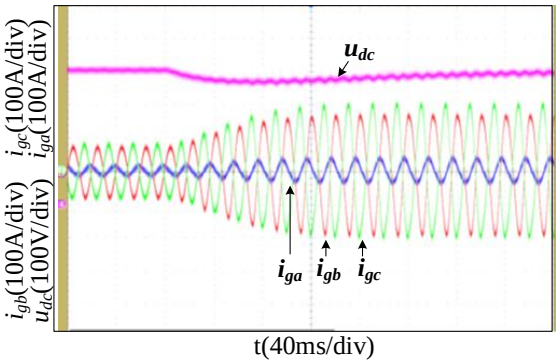

Fig. (11-b) wave of i_{abc} and u_{dc} when dc load increases

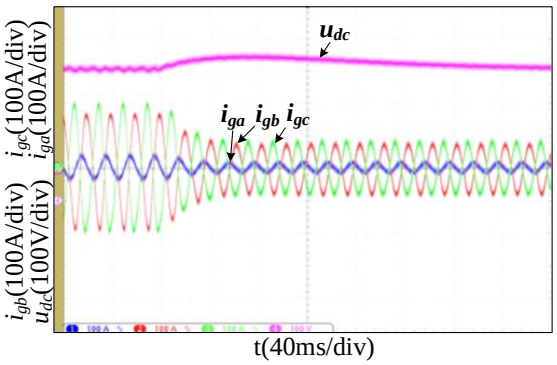

Fig. (11-c) wave of i_{abc} and u_{dc} when dc load decreases

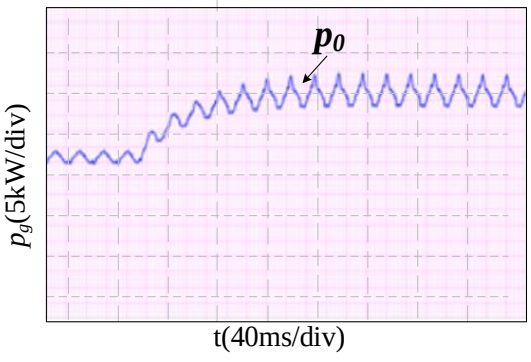

Fig. (11-d) wave of p_0 when dc load increases

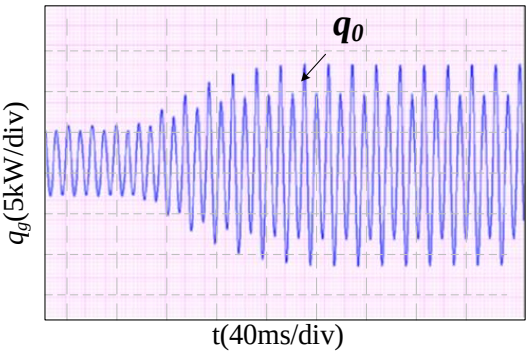

Fig. (11-e) wave of q_0 when dc load increases

Fig.11 dynamic waves with active power fluctuations suppression control

Fig .11 shows the waveforms of the system working on objective of active power fluctuations suppression. At steady state, the phase A current is about 100A smaller than phase B and C. the current is unbalanced because the power fluctuation suppression must be at the cost of injection of negative sequence. The DC-bus voltage is flat because the 100Hz harmonic active power has been suppressed, as Fig. (11-d) shows.

The dynamic response is very fast and steady when dc load increases and decreases both. When dc load increases, DC-bus voltage drops about 40V, but return to the reference value within 300ms. The grid current response time is about 40ms. The input active power increases, leading to that active and reactive power fluctuations both become larger because of the increment of negative sequence current.

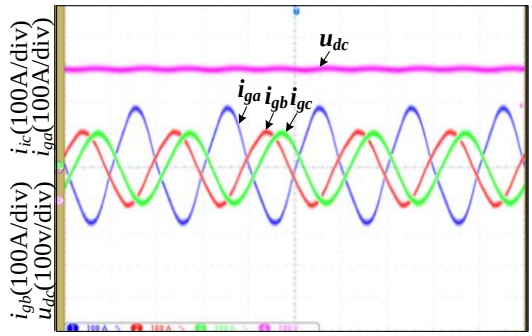

Fig. (12-a) wave of i_{abc} and u_{dc} at steady state

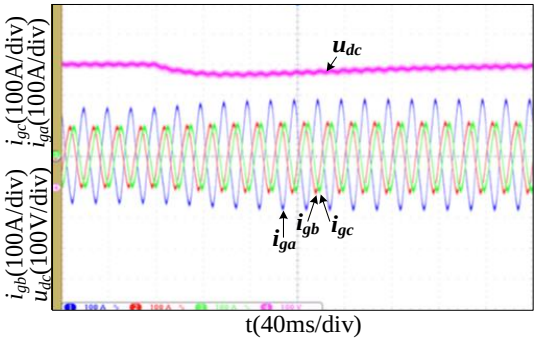

Fig. (12-b) wave of i_{abc} and u_{dc} when dc load increases

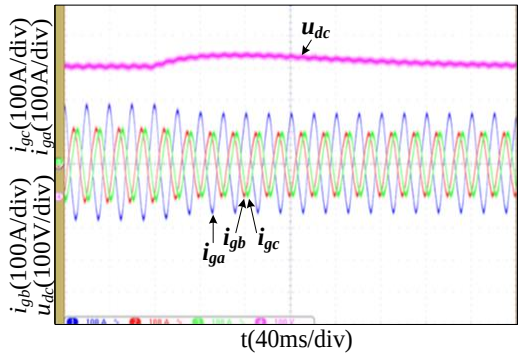

Fig. (12-c) wave of i_{abc} and u_{dc} when dc load decreases

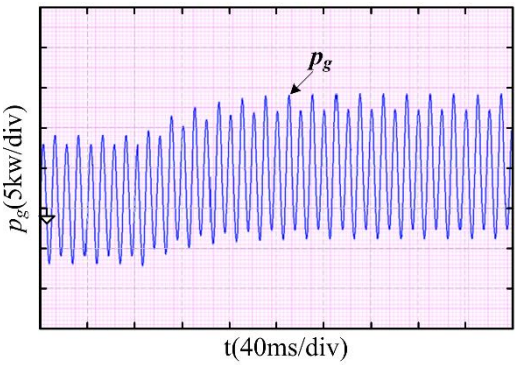

Fig. (12-d) wave of p_0 when dc load increases

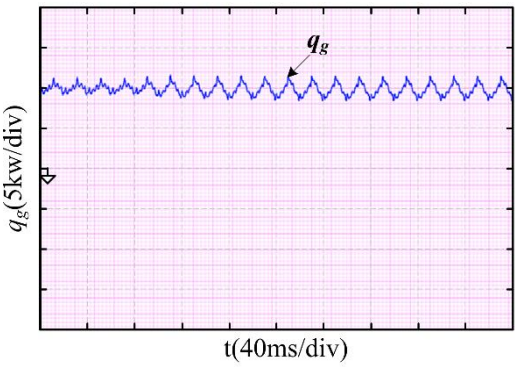

Fig. (12-e) wave of q_0 when dc load increases

Fig.12 dynamic waves with reactive power fluctuations suppression control

Fig .12 shows the waveforms of the system working on objective of reactive power fluctuations suppression. Compared with Fig.11, the DC-bus voltage has more 100Hz harmonic at steady state as (12-a) shows. The current is unbalanced too, and the cause is the same with the former objective. However, phase A current is larger than phase B and C, which is contrary to that in Fig. (11-a).

When dc load increases, the active power fluctuations increase much because this control scheme suppressing 2nd order reactive power cannot restrain the 2nd order active power. The DC-bus voltage rises about 35V and return to steady state within 300ms. While the reactive power in Fig. (12-e) is much flatter than that in Fig. (11-e), which shows this control scheme works on reactive power fluctuations.

6 Conclusion

This paper presents an improved PR control strategy for the wind power generation grid connected inverter under unbalanced grid condition and validates it with simulation and experiments. For the decomposition of the grid voltage positive and negative sequence components, a frequency-adaptive SOGI block with PLL (FA-SOGI-PLL) is proposed. The detailed design of FA-SOGI-PLL is presented. Compared with conventional decomposition method, the FA-SOGI gets a faster response and accurate results. Meantime, to make conventional PR controller able to tune the resonant frequency, this paper implements PR controller on the basis on FA-SOGI, and validates it on a 350kW platform. The results shows that this control scheme has follow advantages: 1) enhanced ability to automatically tune the resonant frequency to adapt to the grid frequency variation, 2) fast dynamic response due to avoiding the current extraction calculation complexity, and 3) good adjustability with different control objectives responding to difference power requirements.

References:

[1] Y. Jun, L. Hui, C. Zhe, X. Xianfeng, C. Xiyin, L. Qing, et al., "Enhanced Control of a DFIG-Based Wind-Power Generation System With Series Grid-Side Converter Under Unbalanced Grid Voltage Conditions," Power Electronics, IEEE Transactions on, vol. 28, pp. 3167-3181, 2013.

[2] F. Mwasilu, J. J. Justo, K. S. Ro, and J. W. Jung, "Improvement of dynamic performance of doubly fed induction generator-based wind turbine power system under an unbalanced grid voltage condition," Renewable Power Generation, IET, vol. 6, pp. 424-434, 2012.

[3] N. Heng, S. Yipeng, Z. Peng, and H. Yikang, "Improved Direct Power Control of a Wind Turbine Driven Doubly Fed Induction Generator During Transient Grid Voltage Unbalance," Energy Conversion, IEEE Transactions on, vol. 26, pp. 976-986, 2011.

[4] C. H. Ng, L. Ran, and J. Bumby, "Unbalanced-Grid-Fault Ride-Through Control for a Wind Turbine Inverter," Industry Applications, IEEE Transactions on, vol. 44, pp. 845-856, 2008.

[5] S. Yongsug and T. A. Lipo, "Control scheme in hybrid synchronous stationary frame for PWM AC/DC converter under generalized unbalanced operating conditions," Industry Applications, IEEE Transactions on, vol. 42, pp. 825-835, 2006.

[6] S. Hong-Seok and N. Kwanghee, "Dual current control scheme for PWM converter under unbalanced input voltage conditions," Industrial Electronics, IEEE Transactions on, vol. 46, pp. 953-959, 1999.
[7] H. Chen, G. Xing, X. Zhou, M. Zhang, and Y. Qu, "Modified direct power control for PWM rectifier under unbalanced grid voltage conditions," in Control Conference (CCC), 2013 32nd Chinese, 2013, pp. 8874-8878.
[8] Y. Meng, W. Gong, S. Hu, and H. Xu, "Control technique on output power quality for doubly fed wind power system," in Power Engineering and Automation Conference (PEAM), 2011 IEEE, 2011, pp. 187-191.
[9] S. Guoqiao, Z. Xuancai, Z. Jun, and X. Dehong, "A New Feedback Method for PR Current Control of LCL-Filter-Based Grid-Connected Inverter," Industrial Electronics, IEEE Transactions on, vol. 57, pp. 2033-2041, 2010.
[10] L. Yanlin and W. Mingyan, "Control stratories for grid-connected and island dualmode operated inverter under unbalanced grid voltage conditions," in Power Electronics and Motion Control Conference (IPEMC), 2012 7th International, 2012, pp. 2152-2156.
[11] H. Jiabing and H. Yikang, "Reinforced Control and Operation of DFIG-Based Wind-Power-Generation System Under Unbalanced Grid Voltage Conditions," Energy Conversion, IEEE Transactions on, vol. 24, pp. 905-915, 2009.
[12] W. Junrui, Z. Yanru, and S. Weizhang, "PR Control for Two-Stage Matrix Converter Excitation Doubly Fed Wind Generation System under Unbalanced Grid Voltage Conditions," in Power and Energy Engineering Conference (APPEEC), 2012 Asia-Pacific, 2012, pp. 1-5.
[13] W. Zhan, N. Heng, and H. Jiabing, "Enhanced Control Strategies of Permanent Magnet Synchronous Wind Power Generation System under Unbalanced Grid Voltage Conditions," in Power and Energy Engineering Conference (APPEEC), 2010 Asia-Pacific, 2010, pp. 1-4.
[14] Rodri, x, P. guez, A. Luna, I. Candela, R. Mujal, et al., "Multiresonant Frequency-Locked Loop for Grid Synchronization of Power Converters Under Distorted Grid Conditions," Industrial Electronics, IEEE Transactions on, vol. 58, pp. 127-138, 2011.
[15] J. Matas, M. Castilla, J. Miret, L. Garcia de Vicuna, and R. Guzman, "An Adaptive Prefiltering Method to Improve the Speed/Accuracy Tradeoff of Voltage Sequence Detection Methods Under Adverse Grid Conditions," Industrial Electronics, IEEE Transactions on, vol. 61, pp. 2139-2151, 2014.
[16] J. G. Hwang and P. W. Lehn, "A Single-Input Space Vector for Control of AC–DC Converters Under Generalized Unbalanced Operating Conditions," Power Electronics, IEEE Transactions on, vol. 25, pp. 2068-2081, 2010.
[17] P. Rodriguez, A. Luna, I. Candela, R. Teodorescu, and F. Blaabjerg, "Grid synchronization of power converters using multiple second order generalized integrators," in Industrial Electronics, 2008. IECON 2008. 34th Annual Conference of IEEE, 2008, pp. 755-760.
[18] F. Gonzalez-Espin, G. Garcera, I. Patrao, and E. Figueres, "An Adaptive Control System for Three-Phase Photovoltaic Inverters Working in a Polluted and Variable Frequency Electric Grid," Power Electronics, IEEE Transactions on, vol. 27, pp. 4248-4261, 2012.